Author's Accepted Manuscript

www.elsevier.com/locate/ijmactool

Sphere forming mechanisms in vibration-assisted ball centreless grinding

Weixing Xu, Dandan Cui, Yongbo Wu

PII: S0890-6955(16)30064-5
DOI: http://dx.doi.org/10.1016/j.ijmachtools.2016.06.004
Reference: MTM3169

To appear in: *International Journal of Machine Tools and Manufacture*

Received date: 17 April 2016
Revised date: 11 June 2016
Accepted date: 14 June 2016

Cite this article as: Weixing Xu, Dandan Cui and Yongbo Wu, Sphere forming mechanisms in vibration-assisted ball centreless grinding, *International Journa of Machine Tools and Manufacture* http://dx.doi.org/10.1016/j.ijmachtools.2016.06.004

Sphere forming mechanisms in vibration-assisted ball centreless grinding

Weixing Xu[1,2], Dandan Cui[3], Yongbo Wu[2,*]

[1] Laboratory for Precision and Nano Processing Technologies, School of Mechanical and Manufacturing Engineering, The University of New South Wales, NSW 2052, Australia

[2] Advanced Machining Technology Laboratory, Department of Machine Intelligence and Systems Engineering, Akita Prefectural University, Akita 0150055, Japan

[3] School of Mechanical & Mining Engineering, The University of Queensland, Queensland 4072, Australia

* Corresponding author: wuyb@akita-pu.ac.jp Tel. (+81 184) 272144

Abstract

This paper aims to clarify the sphere forming mechanisms in vibration-assisted ball centreless grinding, a new technique for effectively processing balls using ultrasonic vibrations. Based on a comprehensive analysis of the ball rotation motion, geometrical arrangement and stiffness of the whole grinding system, a reliable mechanics model was successfully developed for predicting the sphere forming process. Relevant experiments conducted showed that the model had captured the mechanics and the major sphere forming mechanisms in ball centreless grinding. It was found that the ball whole surface can be well ground with a high accuracy, while efficiency is much enhanced compared with that in the traditional methods. The ball rotational speed which is controlled by the ultrasonic regulator has a great impact on final sphericity, and the speed controlled by the ultrasonic shoe dominates the whole processing time. To achieve a stable and high precision grinding, the ball needs to rotate rhythmically, and the wheel feed per step and the ball location angle should be controlled in a critical range.

Keywords:

Ball; Vibration-assisted machining; Centreless grinding; Ultrasonic vibration; Sphere forming mechanisms; Sphericity.

1. Introduction

Spherical components are widely used in many engineering applications, such as balls in bearings [1-3], spherical silicon in photovoltaic energy conversions [4, 5], contact probes in inspection devices and other precision products [6, 7]. To meet the growing demands of high level functional performance, not only the dimensional and geometric control of the balls is strict, but the requirement towards the ball materials is stringent, such as silicon nitride (Si_3N_4), silicon carbide (SiC), aluminium oxide (Al_2O_3) and zirconia (ZrO_2), which are advanced and normally combine with high elastic modulus, hardness and corrosion resistance, low density, friction and thermal expansion coefficient [8]. However, just the abovementioned superior properties bring challenges to the fabrication of advanced balls. As for the processing method, there are mainly two types available: V-groove lapping (VL) and magnetic fluid polishing (MFP). Apparently, the VL methods can be a bit diverse, such as concentric VL, eccentric VL and variable-radius VL, but the balls are normally constrained by the V-shaped groove and revolve around the pad to remove materials [9, 10]. However, the machining cycle usually requires a long considerable time (6-16 weeks) because of the low material removal rate [3, 9-11]. To improve the machining efficiency, MFP was then proposed, which is based on the magneto-hydrodynamic behaviour of a magnetic fluid, and can lower the grinding force and improve the final ball accuracy; nonetheless it is environment-unfriendly and the cycle time also lasts for 20-30 hours [1, 12, 13].

In an attempt to reduce the processing time, the authors have developed a novel grinding technique with the aid of ultrasonic vibration, named vibration-assisted ball centreless grinding [14, 15]. This technique is based on the concept of the ultrasonic vibration-assisted centreless grinding of cylindrical components [16-19]. Two kinds of ultrasonic vibrations are applied to the ball, and by adjusting the directions of the vibrations, the ball can be controlled to rotate in two directions to achieve a full spherical surface grinding [14, 15]. It has been shown that this technique can significantly shorten the processing cycle in grinding of advanced balls. However, the sphere forming mechanisms are still unclear, which has significantly hindered the optimisation and practical application of the new ball grinding technique. The objective of this work is to remove the above barrier through a detailed mechanics analysis to understand the science behind ball centreless grinding, thereby establishing the essential fundamentals.

2. Principle and modelling of ball centreless grinding

2.1 Principle

Fig. 1 illustrates the processing principle of the vibration-assisted ball centreless grinding, in which the ball is placed underneath the grinding wheel and above a ultrasonic shoe with a location angle of α, and constrained by a blade, an ultrasonic regulator and a stop. The grinding wheel rotates at a speed of n_g and feeds in at a speed of V_{fr}. The material removal starts as the wheel interferes with the ball. Once the required stock removal Δ has been attained, the wheel feeding will stop followed by a dwell to allow "spark-out". During grinding, the ball's rotation around z-axis is controlled by the elliptic vibration from ultrasonic shoe, which is a typical centreless grinding operation for high precision roundness forming [16-19]. With an additional well-controlled rotational motion around x-axis by ultrasonic regulator, the whole surface of the ball can be well ground to generate a spherical shape. To do this, a stop is arranged to work under a pressure of F to provide sufficient control force through friction between the ball and regulator. Suppose the ultrasonic shoe and regulator vibrate at frequencies of f_s and f_r, and amplitudes of A_s and A_r, their corresponding vibration velocities, v_s and v_r, can be described as

$$\begin{cases} v_s(t) = 2\pi f_s A_s \sin(2\pi f_s t) \\ v_r(t) = 2\pi f_r A_r \sin(2\pi f_r t) \end{cases} \tag{1}$$

For a precision control, the tangential velocities of the ball rotation around z and x-axis are the same as the maximum vibration speeds of the ultrasonic shoe and regulator, respectively [14, 15]. Therefore, the ball rotational speed around z-axis and x-axis becomes

$$\begin{cases} n_{wz} = 2\pi f_s A_s / d_w \\ n_{wx} = 2\pi f_r A_r / d_w \end{cases} \tag{2}$$

where d_w is the ball diameter.

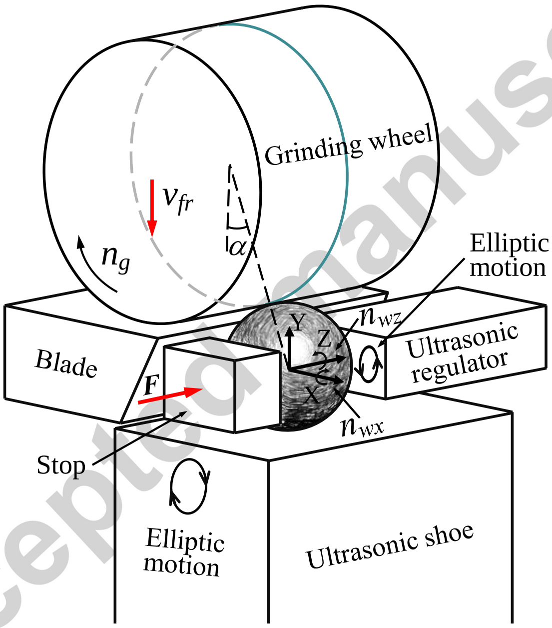

Fig. 1 An illustration of vibration-assisted ball centreless grinding.

2.2 Modelling

Fig. 2 shows the geometrical arrangement of the ultrasonic shoe, blade, regulator, stop, ball and grinding wheel in ball centreless grinding after machining for time t, by which the ball location angle and radius at the grinding point A become $\alpha(t)$ and $\rho(t)$, respectively, from their initial values of α_0 and ρ_0. The blade has a tilt angle of ϕ. In order to establish the mechanics model for ball centreless grinding, several assumptions are made: (1) the ball is in constant contact with the blade, shoe, stop and regulator at points B, C and D, during grinding; (2) the vibration of the entire machine is too small to be regarded, and no chatter occurs on the machine due to the ultrasonic vibration of the shoe and regulator; (3) the ball rotational speed around x-axis and z-axis are always stable; (4) the wear of the grinding wheel is too small to be recognized, and the grinding wheel radius R_g is kept constant during grinding.

As shown in Fig. 2, let a xyz-coordinate system be located on the grinding apparatus: the z-axis is assigned along the axial direction of wheel, the y-axis in vertical direction, and the x-axis in parallel with the end-face of grinding wheel. Before grinding, the initial xyz-coordinates of the grinding wheel centre O_{g0} and the ball centre O_{w0} are (X_{Og0}, Y_{Og0}, Z_{Og0}) and (X_{Ow0}, Y_{Ow0}, Z_{Ow0}), respectively. The contact point B_0 (X_{B0}, Y_{B0}, Z_{B0}), C_0 (X_{C0}, Y_{C0}, Z_{C0}) and D_0 (X_{D0}, Y_{D0}, Z_{D0}) then can be obtained from the initial geometrical arrangement, as follows:

$$\begin{cases} X_{B0} = X_{Ow0} - \rho_0 \sin\phi \\ Y_{B0} = Y_{Ow0} + \rho_0 \cos\phi \\ Z_{B0} = Z_{Ow0} \end{cases} \quad \begin{cases} X_{C0} = X_{Ow0} \\ Y_{C0} = Y_{Ow0} - \rho_0 \\ Z_{C0} = Z_{Ow0} \end{cases} \quad \begin{cases} X_{D0} = X_{Ow0} \\ Y_{D0} = Y_{Ow0} \\ Z_{D0} = Z_{Ow0} + \rho_0 \end{cases} \tag{3}$$

The planar equations representing the contact faces of the ball with blade, ultrasonic shoe and regulator can be written as:

The equation for ball-blade contact face is

$$Y - Y_{B0} = \tan\phi (X - X_{B0}) \tag{4a}$$

for ball-shoe contact face is

$$Y - Y_{C0} = 0 \tag{4b}$$

and for ball-regulator contact face is

$$Z - Z_{C0} = 0 \tag{4c}$$

Substituting coordinates of the points B and C into Eqs. 4a and b, respectively, gives

$$PX + QY + R = 0 \tag{5}$$

$$Y - Y_{Ow0} + \rho_0 = 0 \tag{6}$$

where

$$\begin{cases} P = \tan\phi \\ Q = -1 \\ R = Y_{Ow0} + \rho_0 \cos\phi - \tan\phi(X_{Ow0} - \rho_0 \sin\phi) \end{cases}$$

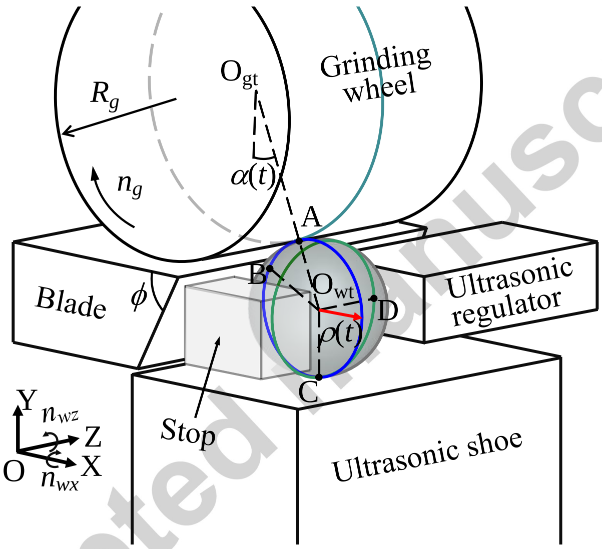

Fig. 2 Geometrical arrangement in ball centreless grinding.

During grinding, the coordinates of the ball centre O_{wt} and the grinding wheel centre O_{gt} will vary as material is removed. Let the instantaneous ball radius in the direction be parallel to the *x*-axis after grinding for time *t* be $\rho(t)$ (see Fig. 2). At this moment, the ball radius at points A, B and C become $\rho_A(t)$, $\rho_B(t)$ and $\rho_C(t)$, respectively. Because of the material removal, $\rho_B(t)$ and $\rho_C(t)$ vary with the grinding processing. However, they are equal to the distances from the ball centre O_{wt} to the blade end-face |OB| and to the shoe end-face |OC|, respectively. Thus,

$\rho_B(t)$ and $\rho_C(t)$ can be described as follows:

$$\rho_B(t) = \frac{|PX_{Ow}(t) + QY_{Ow}(t) + R|}{\sqrt{P^2 + Q^2}} \tag{7}$$

$$\rho_C(t) = Y_{Ow}(t) - Y_{Ow0} + \rho_0 \tag{8}$$

Solving Eqs. (7) and (8) simultaneously can yield *x* and *y* coordinates of the ball centre O_{wt} at time *t*.

$$\begin{cases} X_{Ow}(t) = [\sqrt{P^2 + Q^2}\rho_B(t) - QY_{Ow}(t) - R] \big/ P \\ Y_{Ow}(t) = \rho_C(t) + Y_{Ow0} - \rho_0 \end{cases} \tag{9}$$

At this moment, the coordinates of the grinding wheel centre O_{gt} become

$$\begin{cases} X_{Ogt} = X_{Og0} = X_{Ow0} - (R_g + \rho_0)\sin\alpha \\ Y_{Ogt} = Y_{Og0} - i\delta = Y_{Ow0} + (R_g + \rho_0)\cos\alpha - i\delta \qquad \delta(i-1)T < t < iT \\ Z_{Ogt} = Z_{Ow}(t) = Z_{Ow0} + \rho_0 - \rho_D(t) \end{cases} \tag{10}$$

where δ is the wheel feeding distance in a single step, *i* (=1, 2, 3…) is the step number and *T* is the time required for the whole revolution of the ball. Therefore, the following relationships can be established.

$$\begin{cases} [X_A(t) - X_{Og}(t)]^2 + [Y_A(t) - Y_{Og}(t)]^2 = R_g{}^2 \\ Y_A(t) - Y_{Ow}(t) = \cot\alpha(t)[X_A(t) - X_{Ow}(t)] \end{cases} \tag{11}$$

where

$$\cot\alpha(t) = \frac{[Y_{Og}(t) - Y_{Ow}(t)]}{[X_{Og}(t) - X_{Ow}(t)]} \tag{12}$$

Subsequently, the grinding point A at time *t* can be obtained by re-arranging Eqs. (11) and (12).

$$\begin{cases} X_A(t) = \dfrac{-V - \sqrt{V^2 - 4UW}}{2U} \\ Y_A(t) = \cot\alpha(t)[X_A(t) - X_{Ow}(t)] + Y_{Ow}(t) \\ Z_A(t) = Z_{Ow0} + \rho_0 - \rho_D(t) \end{cases} \tag{13}$$

where

$$\begin{cases} U = 1 + \cot^2 \alpha(t) \\ V = 2[\cot \alpha(t) Y_{Ow}(t) - \cot^2 \alpha(t) X_{Ow}(t) - \cot \alpha(t) Y_{Og}(t) - X_{Og}(t)] \\ W = X_{Og}{}^2(t) + [\cot \alpha(t) X_{Ow}(t) - Y_{Ow}(t) + Y_{Og}(t)]^2 - R_g{}^2 \end{cases},$$

Eventually, the ball radius $\rho_A(t)$ at point A after grinding for time t can be calculated using the coordinates of the ball center O_{wt}.

$$\rho_A(t) = \sqrt{[X_A(t) - X_{Ow}(t)]^2 + [Y_A(t) - Y_{Ow}(t)]^2} \tag{14}$$

Consequently, the apparent wheel depth of cut would be $\eta' = \rho(t-T_A-T) - \rho(t-T_A)$, where T_A is the time required for one revolution of the ball around z-axis. If the grinding system has an ideal stiffness, the true wheel depth of cut would be equal to the apparent one. However, the grinding system withstands the elastic deformation caused by the grinding force during actual grinding. To indicate the elastic deformation of centreless grinding system, Rowe *et al*. introduced a dimensionless parameter called machining elasticity parameter k, which is defined as a quotient between the true depth of cut and the apparent depth of cut with Eq. (15) [16, 20].

$$k = \frac{\text{true wheel depth of cut}}{\text{apparent wheel depth of cut}} = \frac{\eta}{\eta'} \tag{15}$$

Therefore, the true wheel depth of cut η becomes $\eta = k\eta'$, and the ball radius at point A can be described as

$$\rho_A(t) = \rho_A(t-T) - k\{\rho_A(t-T) - \sqrt{[X_A(t) - X_{Ow}(t)]^2 + [Y_A(t) - Y_{Ow}(t)]^2}\} \tag{16}$$

Considering the wheel depth of cut calculated by these equations is occasionally less than zero, which would not happen. Eq. (16) then needs to be modified as

$$\begin{cases} \rho_A(t) = \rho_A(t-T) - k(\rho_A(t-T) - \sqrt{[X_A(t) - X_{Ow}(t)]^2 + [Y_A(t) - Y_{Ow}(t)]^2}) & \\ & \rho_A(t) \le \rho_A(t-T) \\ \rho_A(t) = \rho_A(t-T) & \rho_A(t) > \rho_A(t-T) \end{cases} \tag{17}$$

2.3 Determination of the machining elasticity parameter

As discussed above, the machining elasticity parameter k depends on the stiffness of the grinding system. If the simulation result is to be trusted, the value of k should be determined for the given grinding system. Since the cutting performs only in xy-plane, for simplify, the spark-out stage without rotational motion around x-axis (n_{wx}=0) was investigated to deduce the parameter k. Suppose the apparent wheel depth of cut is removed just after a few revolutions of ball, the decrease rate of the wheel depth of cut depends on the value of parameter k. If the apparent wheel depth of cut has a value of a_0 at the beginning of spark-out, the true depth of cut in the first half-revolution, a_1, and that in the second half-revolution, a_2, can be deduced by the following equations.

$$a_1 = ka_0 \tag{18}$$

$$a_2 = k(a_0 - a_1) = (1-k)a_1 \tag{19}$$

Hence, the true depth of cut in the ith half-revolution, a_i, can be obtained as:

$$a_i = k(a_0 - a_1 - a_2 - ... - a_{i-1}) = (1-k)^{i-1} a_1 = \ldots = (1-k)^{i-m} a_m \quad (m = 1, 2, \cdots, i) \tag{20}$$

Since the true depth of cut is proportional to the normal grinding force F_n, the following relationship is then obtained:

$$\frac{F_{ni}}{F_{nm}} = \frac{a_i}{a_m} = (1-k)^{i-m} \tag{21}$$

where F_{ni} and F_{nm} are the normal grinding forces in ith and mth half-revolution of the workpiece for spark-out. Solving Eq. (21) yields

$$k = 1 - e^{\lambda} \tag{22}$$

where e is the base of natural logarithms and $\lambda=(\ln F_{ni}-\ln F_{nm})/(i-m)$. Consequently, the value of k can be determined as long as forces F_{ni} and F_{nm} are known by measurements. As illustrated in Fig. 3a, let F_x and F_y be the cutting forces in x- and y- directions, respectively. Based on the geometrical arrangement, the following relationship can be obtained:

$$\begin{cases} F_n \cos\alpha + F_t \sin\alpha = F_y \\ F_n \sin\alpha - F_t \cos\alpha = F_x \end{cases} \tag{23}$$

where F_t is the tangential grinding force. Solving Eq. (23) yields

$$F_n = F_y \cos\alpha + F_x \sin\alpha \tag{24}$$

Therefore, the normal grinding force F_n can be obtained as long as the value of F_x and F_y are known, and then the value of parameter k can be determined using Eq. (20).

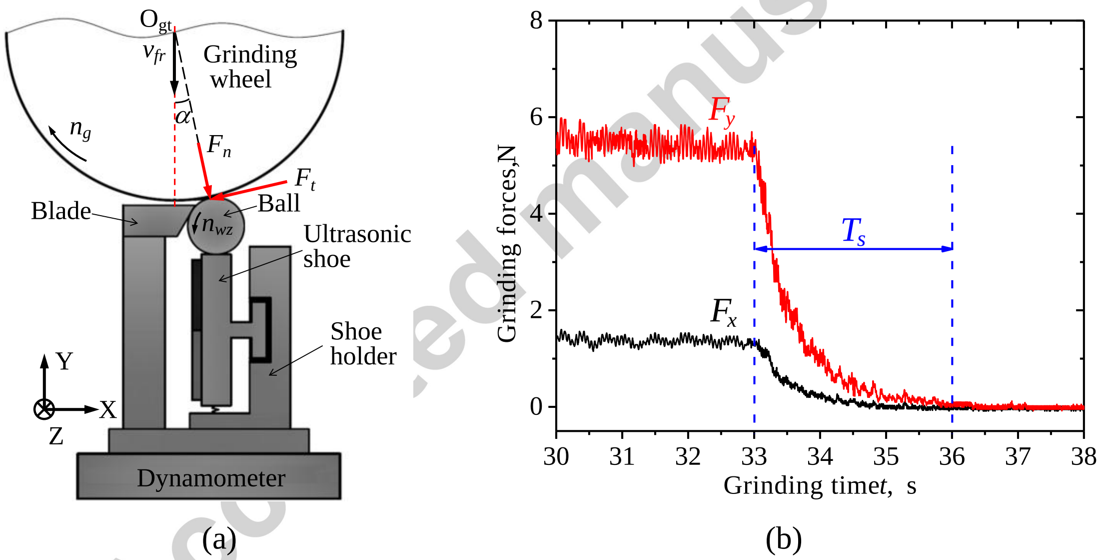

Fig. 3 Measurement of the grinding forces: (a) illustration and (b) force result.

To get the machining elasticity parameter, a grinding test was then carried out on the proposed grinding system, in which the ultrasonic regulator was stopped for the performing of the grinding discussed above. The grinding forces F_x and F_y in the horizontal and vertical directions were recorded by a dynamometer (model type 9256A1, Kistler Ltd.), as shown in Fig. 3a. The set depth of cut was Δ=18μm with a spark-out time of T_s=3s. The ball located angle was α=3° and the wheel feed rate was v_{fr}=0.6μm/s. The obtained grinding forces are shown in Fig. 3b. Obviously, the forces decrease rapidly as the feed-in is stopped to allow the spark-out to take place. The values of F_{ni} and F_{nm} then can be calculated using Eqs. (23) and (24) by the data F_{xi}, F_{xm}, F_{yi}, F_{ym}, and consequently the parameter k=0.14 was obtained with Eq. (22).

3. Grinding conditions for model prediction and experiment

The experimental setup and power supply system for ball centreless grinding is shown in Fig. 4. The ultrasonic shoe and regulator are constructed by bonding a piezoelectric ceramic device (PZT) with two and four separated electrodes onto a metal elastic body, respectively. When the two alternative current (AC) signals with a phase difference generated by wave function generator are applied to the PZT after being amplified by means of power amplifiers, bending and longitudinal ultrasonic vibration are excited simultaneously. The synthesis of the vibration displacements in the two directions creates an elliptic motion on the end-faces of the metal elastic body [16, 17, 19]. The rotations of the ball around z-axis and x-axis are controlled through the frictional force between the ball and metal elastic body, respectively. In addition, the blade is wedge-shaped with a tilt angle of 60° in terms of the optimum workpiece rounding condition demonstrated by Harrison and Pearce [21].

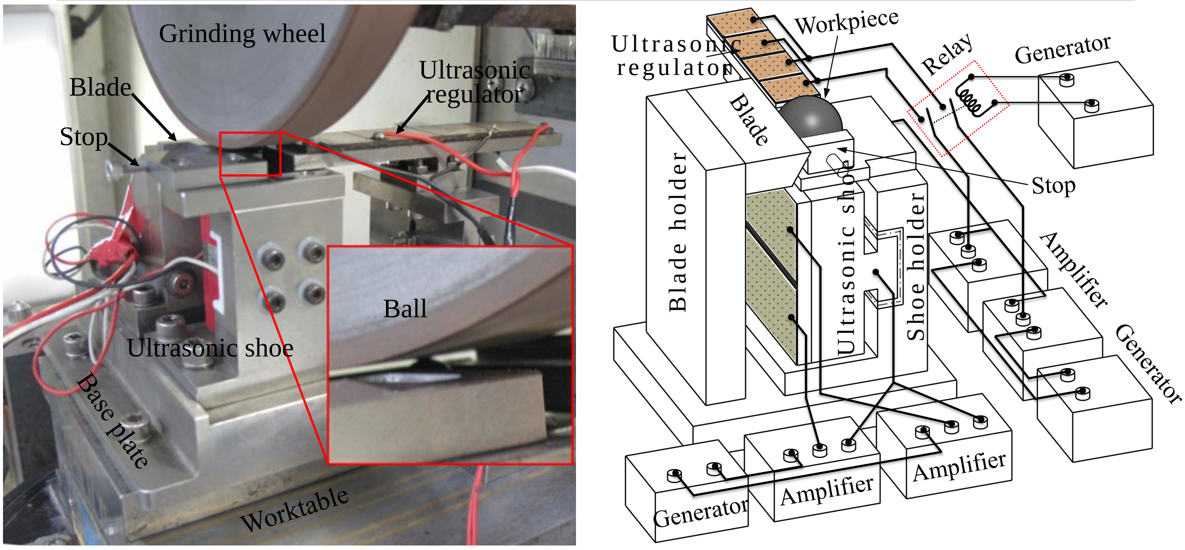

(a) (b)

Fig. 4 (a) Experimental setup and (b) power supply system for ball centreless grinding.

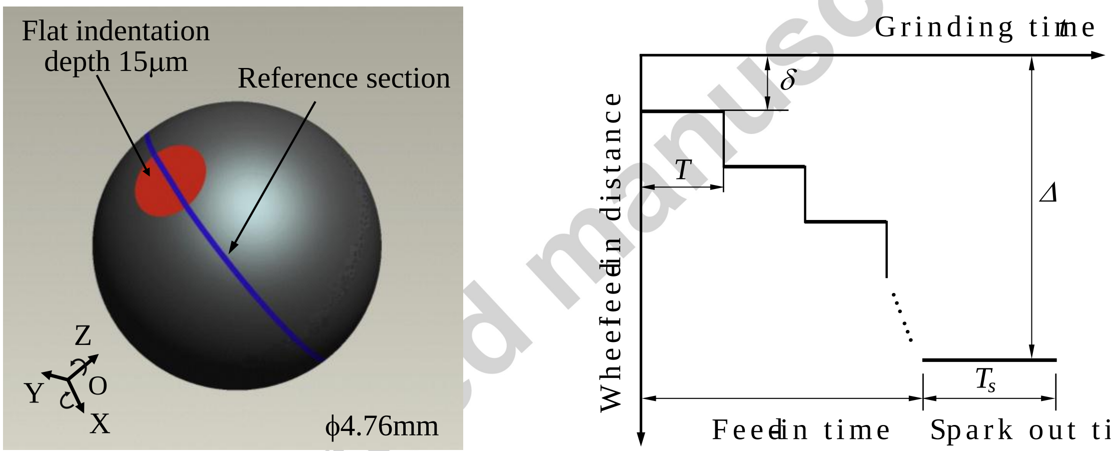

(a) (b)

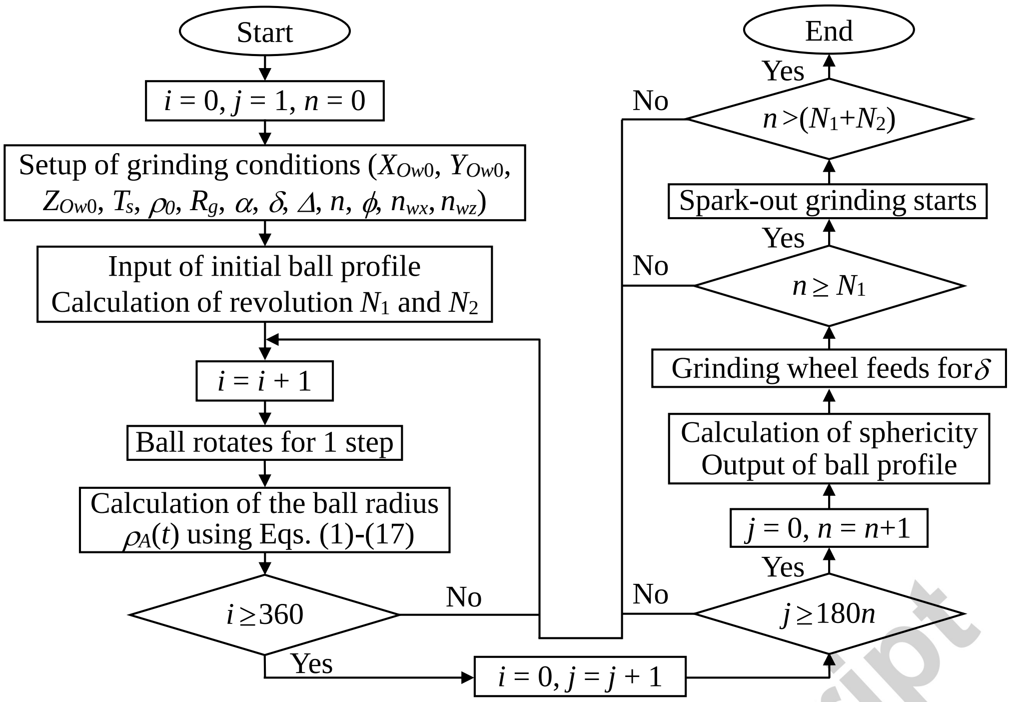

(c)

Fig. 5 (a) Initial workpiece profile, (b) grinding wheel feeding method, and (c) program flowchart for simulation.

A silicon nitride (Si_3N_4) ball with a diameter of 4.76mm, shown in Fig. 5a, was used for simulation and experiments. A flat indentation with depth of 15µm in the radial direction was generated on its circumference to indicate the initial ball surface. The reason for using such an initial shape is that a flat indentation can be prepared easily and any lack of centreless grinding process to eliminate a certain order of waviness would be readily indicated, since the shape already contains an appreciable contribution to all the important orders [22]. A #1500 grit synthetic diamond wheel (SDC1500N75B, D180 T15 H31.75) was adopted as the grinding tool. After grinding, the roundness was measured with a roundness measurement instrument (Rondcom55A by Tokyo Seimitsu Co., Ltd.) at six different cross-sections which interlaced with each other, and the average value of the measurements was used to indicate the ball sphericity.

In simulation, to describe the ball profile, a reference section was selected as highlighted in Fig. 5a. The ball was divided at an interval of one degree around *x*-axis, and also one degree for each section around its centre. Therefore, the ball could be divided into 180 sections around *x*-axis, and 360 segments for each section. Suppose the workpiece initial profile can be described with radius of $\rho(j, i)$, then i=1-360 and j=1-180. In any given time t during grinding, as long as $\rho_B(t)$ and $\rho_C(t)$ are known, the instantaneous radius of $\rho_A(t)$ can be calculated using the Eqs. (1) - (17). Following the flowchart in Fig. 5c, the grinding process was divided into two stages (see Fig. 5b). In the first stage, the wheel fed into the ball with a step by step feed δ, following by a dwell for time T, during which the ball rotated around *z*- and *x*-axis separately for a whole spherical surface grinding; when the wheel reached its final position after rotating $N_1(=\Delta T n_{wz}/\delta)$ revolutions, the second stage started, in which the wheel stopped feeding for spark-out process for time T_s (workpiece rotated for $N_2=n_{wz}T_s$ revolutions). To achieve the same grinding operation, a relay, which was controlled by a wave generator, was connected in series with amplifiers in the experimental setup. As shown in Fig. 4b, when the switch was "on", the ball started rotating around *x*-axis, and stopped when the switch turned to "off", during which a typical centreless grinding was performed around *z*-axis [23-26]. Thus, the grinding wheel will stop for a duration of $T_{off}/(n_{wx}T_{on})+1/n_{wx}$ after each step feeding for performing a cycle of ball whole surface grinding. Additionally, Table 1 outlines the parameters for model prediction and experiments.

Table 1 Simulation and experimental conditions.

Grinding wheel radius R_g [mm]	90
Initial workpiece radius ρ_0 [mm]	2.38
Blade angle ϕ [°]	60
Location angle α [°]	0-9
Wheel feed rate v_{fr} [μm/s]	0.6

Wheel rotational speed n_g [rpm]	2200
Wheel feeding per step δ [μm]	1-14
Wheel feeding depth Δ [μm]	28
Ball rotational speed n_{wz} [rpm]	120
Ball rotational speed n_{wx} [rpm]	3
Relay switching "on" time T_{on} [s]	0.01-0.38
Relay switching "off" time T_{off} [s]	0.5-2.5
Machining elasticity parameter k	0.14
Spark-out time T_s [s]	180

4. Results and discussion

4.1 Sphere forming

Fig. 6 shows the variation of the ball surface and sphericity E_s during grinding in simulation under the conditions of Δ=28μm, δ=2μm, α=3°, T_s=180s, T_{on}=0.11s and T_{off}=0.5s. As the size of the initial flat indentation decreases gradually, some new comparatively small convex and concave areas formed at the beginning, but the following grinding process decreases the height of these areas, which eventually improves the ball sphericity. It can be seen that the sphericity error E_s tends to monotonously decrease during grinding, and finally it reaches 0.92μm from its initial value of 15.0μm after a spark-out of 180s.

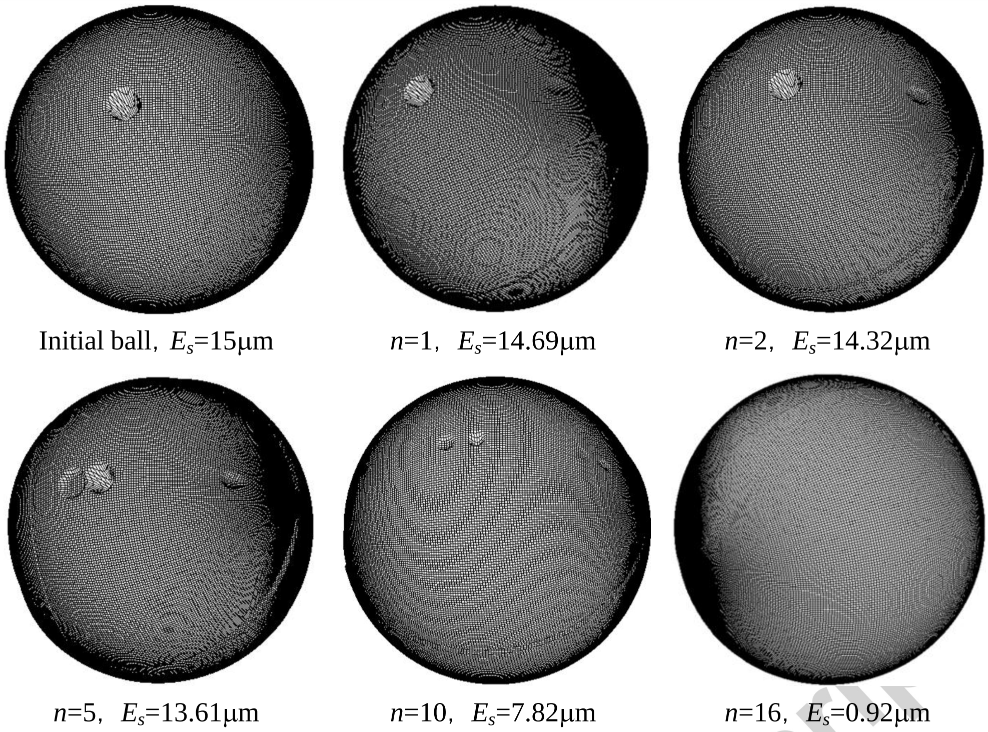

(a)

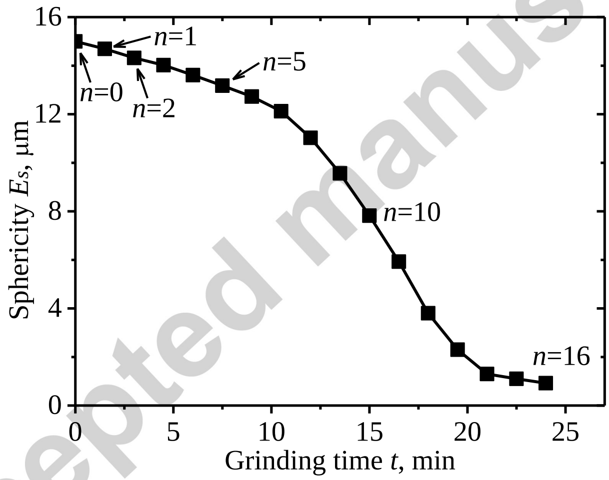

(b)

Fig. 6 Variation of (a) ball profile and (b) sphericity during grinding.

Fig. 7a shows two typical cross-sections of the ball: one crosses the flat place, and the other is vertical to the first section. The variation of the cross-section profiles and roundness can be found in Figs. 7b. It is obvious that the roundness variation tendency of the cross-section in the flat area is similar to that of ball sphericity (see Fig. 6b). However, to fit the new sphere surface, the roundness error of cross-section 2 increases first and then decreases with that of the section passing through the flat area during grinding.

Figs. 8a and b show the images and cross-section profiles of workpiece before and after grinding under the same conditions with experiment. It can be seen that the flat indentation on the initial workpiece was eliminated and the workpiece cross-section roundness was greatly improved from its initial value of 13.25μm to 0.78μm (the sphericity was about 0.84μm), consequently validating the proposed ball centreless grinding technique and simulation model.

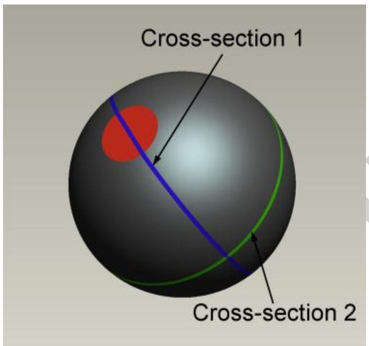

(a)

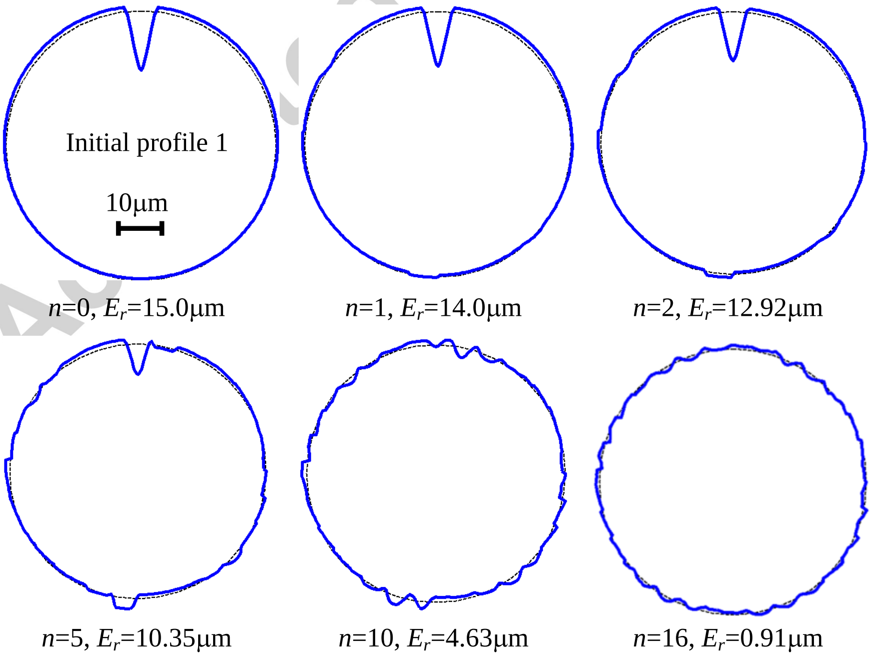

(b)

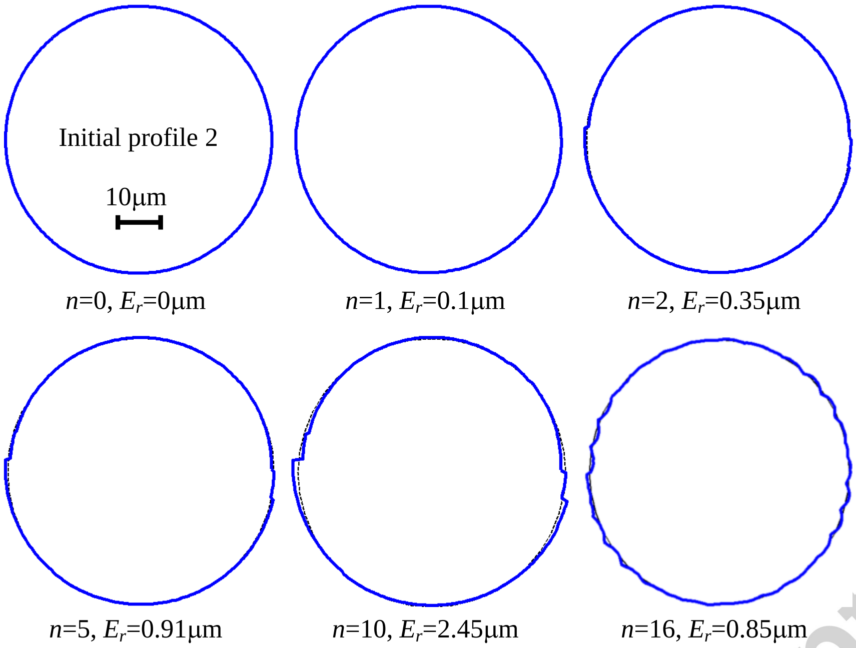

(c)

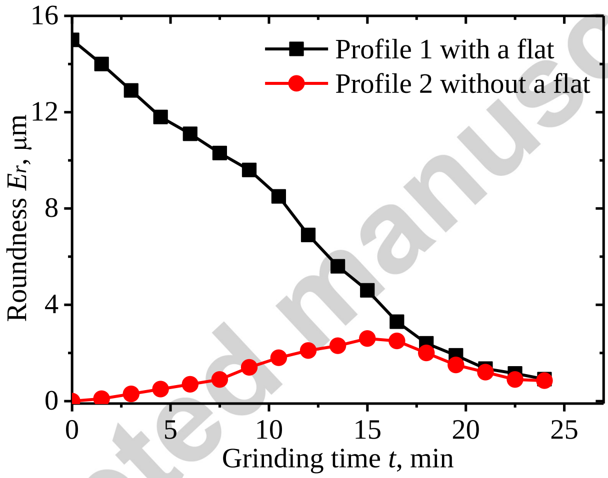

(d)

Fig. 7 (a) Location of the selected cross-sections, and variation of the profiles for (b) cross-section 1 and (c) cross-section 2, and (d) their roundness during grinding.

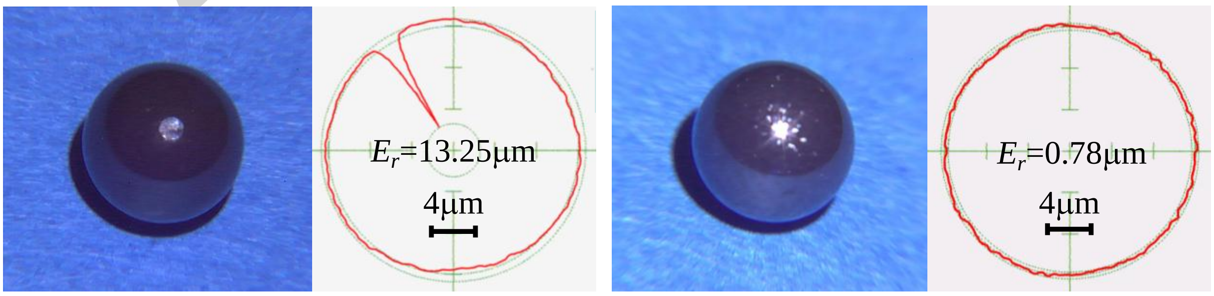

(a) (b)

Fig. 8 Snapshots of ball workpiece and surface profiles before (a) before grinding and (b) after grinding.

4.2 Rotation control

Obviously, increasing the ball rotational speed could reduce the whole processing period. However, to achieve a high accuracy, a well-controlled ball rotation motion is essential. To do this, except the ultrasonic shoe and regulator, a relay was plugged in to the power supply system as well (see Fig. 4b). It is obvious that the switch "off" time T_{off} greatly affects the roundness of the cross-sections passing through x-axis [18], while the switch "on" time T_{on} determines the whole ground area on spherical surface. To well-grind the whole ball surface, T_{off} should be an integral number of the ball rotation period ($1/n_{wz}$) around z-aixs, while T_{on} should be small enough.

To investigate the effect of T_{on} on the final ball quality, simulation prediction and grinding operation were both carried out under the same condition of T_{off}=1/n_{wz}=0.5s. As shown in Fig. 9a, the time T_{on} affects the ball sphericity E_s significantly. E_s decreases with the increase of time T_{on} at the beginning till its valley value at 0.11s with a sphericity of 0.82μm, and then switches to increase afterwards. The reason can be clearly seen from the simulation results (red dots): a short time T_{on} results in a minor rotation angle around x-axis, whereas a long time T_{on} could easily cause a discontinuous grinding. However, in an actual grinding operation, the ball needs a short time to start motion for each step. Therefore, for a well ground ball, the relay switching "on" time needs to be controlled in a suitable range, and it is between 0.1s and 0.2s for the proposed system. The effect of T_{off} is shown in Fig. 9b, in which T_{off} changes from 1/n_{wz}(=0.5s) to 5/n_{wz}(=2.5s), while T_{on} is constant at 0.11s. Obviously, the time T_{off} does not affect the sphericity as much as T_{on} does. This is because except the first revolution the rest are equivalent to the grinding in spark-out stage, in which the roundness/sphericity decreases a little bit, similar to those shown in Figs. 6b and 7d.

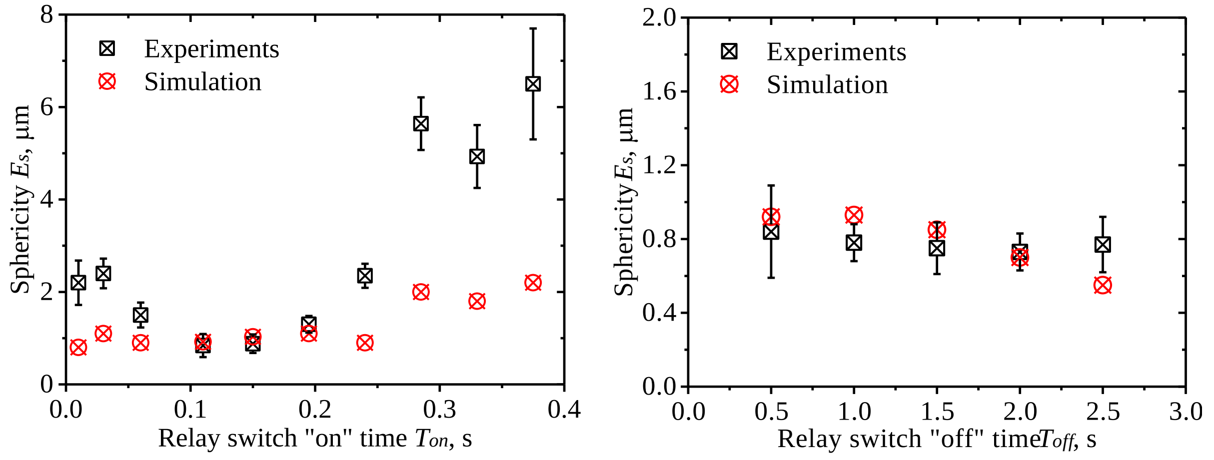

(a) (b)

Fig. 9 Effects of relay switch (a) "on" and (b) "off" time on ball sphericity.

4.3 Sphericity

Under the condition of T_{on}=0.11s and T_{off}=0.5s, both the simulation prediction and experiments were performed to investigate the effect of the core factors (i.e., wheel feed per step and ball location angle) on the final sphericity. The influence of the wheel feed per step, δ, is shown in Fig. 10a. As can be seen, the sphericity decreases with the decrease of δ and comes to 0.75μm when δ=1μm, however, it costs double processing time compared with that with δ=2μm. It is also possible to shorten the grinding time by increasing the feed per step for the same sphericity. But to do this, the ball rotational speed must be large enough to achieve an adequate number of revolutions, due to the cross-section roundness correction is directly related to the number [23, 26]. As discussed in Eq. (2) and [14], the high ball rotational speed can be obtained by increasing the voltage or frequency that was applied on the vibrators. Moreover, due to the instability of the ball rotation motion caused by the large δ, (e.g., δ=14μm) the gap between the simulation prediction and experimental results is enlarged. Fig. 10b shows the variation of the ball sphericity under different location angle, α. It is obvious that to achieve a high accuracy, the ball should be located in a certain working zone, and its location angle for the proposed system is 2-6°. In addition, since the grinding, the ball located right below the wheel, is no longer following the criteria of 3-point contact for centreless grinding [23-25], thus the sphericity for α=0° was quit poor and unstable.

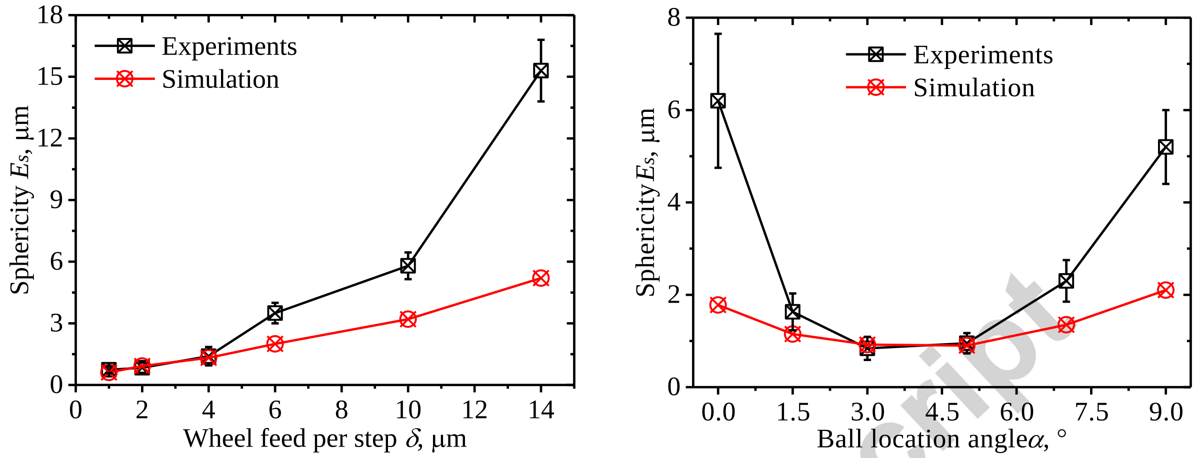

(a) (b)

Fig. 10 Effects of (a) wheel feed per step and (b) ball location angle on sphericity.

5. Conclusions

To clarify the sphere forming process in the vibration-assisted ball centreless grinding, this paper successfully established a mechanical model. The capability of the model has been verified by experiments. The results from the simulation and experiments bring about the following major conclusions:

(1) The whole surface of the ball can be well ground under the control of two ultrasonic vibrations via the frictions between the ball and vibrators. The proposed grinding setup has been proved to possess the capability of achieving a high accuracy at a large material removal rate, and it enables the whole process shortened to be less than half an hour. Yet, the machining efficiency could be further improved by increasing the vibration amplitude or frequency.

(2) The ball rotational speed, which is controlled by the ultrasonic regulator, has a great

impact on ball sphericity, while the speed controlled by the ultrasonic shoe dominates the whole processing time. To achieve a high accuracy, the wheel feed per step should be small enough (i.e., less than 6μm) and the ball needs to be placed in an effective location angle (i.e., 2-6°).

(3) To rhythmically control the ball rotation motion vertical to the grinding wheel, a relay is connected in series with ultrasonic regulator in power supply system. For a stable and high precision grinding, its switch-closing/opening time needs to be controlled in a critical range.

Acknowledgement

This research was financially supported in part by Micron Machinery Co., Ltd.. The authors also gratefully acknowledge the financial support from the Osawa Scientific Studies Grants Foundation and the Grants-in-Aid for Science Research from the Japan Society for the Promotion of Science (Grant No. 17560100). The Authors also would like to thank Prof. Liangchi Zhang from The University of New South Wales for his support on this work.

Nomenclature

PZT	piezoelectric ceramic	T_A	time for ball rotates one revolution around z-axis, s
AC	alternative current	T_{off}	relay switch off time during wheel feed-in, s
VL	V-groove lapping	T_{on},	relay switch on time during wheel feed-in, s
MFP	magnetic fluid polishing	T_s	spark-out time, s
a_0	apparent wheel depth of cut at the beginning of spark-out	v_s, v_r	vibration velocities on top of shoe and regulator, m/s

a_i, a_m	true depth of cut in the *i*th/*m*th half-revolution in spark-out	V_{fr}	grinding wheel feed rate, μm/s
A_s, A_r	applied vibration amplitudes on shoe and regulator, μm	α_0	ball initial location angle, °
d_w	ball diameter, mm	$\alpha(t)$	ball location angle at time *t*, °
E_r	roundness of the measured cross-section, μm	δ	wheel feeding step, μm
E_s	ball sphericity error, μm	Δ	wheel feeding depth, μm
f_s, f_r	applied vibration frequencies on shoe and regulator, kHz	ρ_0	ball initial radius, mm
F_n, F_t	normal and tangential grinding force	$\rho(t)$	ball radius at time *t*, mm
F_x, F_y	grinding force in *x*- and *y*-directions	$\rho_A(t)$, $\rho_B(t)$, $\rho_C(t)$	ball radius at contact points A, B and C after grinding for time *t*
F	pressure force on stoper, N	ϕ	blade angle
k	machining elasticity parameter of the grinding system	O_g (X_{Og}, Y_{Og}, Z_{Og})	coordinates of grinding wheel centre
n_g	grinding wheel rotational speed, rpm	O_w (X_{Ow}, Y_{Ow}, Z_{Ow})	coordinates of ball centre
n_{wz}, n_{wx}	ball rotational speed around *z*-axis and *x*-axis, rpm	A (X_A, Y_A, Z_A)	coordinates of grinding point A
N_1, N_2	ball revolution number before and after spark-out process	B (X_B, Y_B, Z_B)	coordinates of contact point B
R_g	grinding wheel radius, mm	C (X_C, Y_C, Z_C)	coordinates of contact point C
T	grinding period time, s	D (X_D, Y_D, Z_D)	coordinates of contact point D

References

[1] N. Umehara, T. Kirtane, R. Gerlick, V.K. Jain, R. Komanduri, A new apparatus for finishing large size/large batch silicon nitride(Si3N4) balls for hybrid bearing applications by magnetic float polishing (MFP), Int J Mach Tool Manu, 46 (2006) 151-169.

[2] W.Z. Ma, B. Zhang, A. Nakajima, T. Mawatari, Electrolytic in-process dressing grinding of ceramic balls, Int J Adv Manuf Tech, 79 (2015) 1153-1160.

[3] F. Zhou, J. Yuan, B. Lyu, W. Yao, P. Zhao, Kinematics and trajectory in processing precision balls with eccentric plate and variable-radius V-groove, The International Journal of Advanced Manufacturing Technology, (2015) 1-12.

[4] T. Maruyama, H. Minami, Light trapping in spherical silicon solar cell module, Sol Energ Mat Sol C, 79 (2003) 113-124.

[5] T. Minemoto, M. Murozono, Y. Yamaguchi, H. Takakura, Y. Hamakawa, Design strategy and development of spherical silicon solar cell with semi-concentration reflector system, Sol Energ Mat Sol C, 90 (2006) 3009-3013.

[6] P.A. Cauchick-Miguel, T.G. King, Factors which influence CMM touch trigger probe performance, Int J Mach Tool Manu, 38 (1998) 363-374.

[7] P.I. Ro, W. Shim, S. Jeong, Robust friction compensation for submicrometer positioning and tracking for a ball-screw-driven slide system, Precis Eng, 24 (2000) 160-173.

[8] R. Komanduri, Z.B. Hou, N. Umehara, M. Raghunandan, M. Jiang, S.R. Bhagavatula, A. Noori-Khajavi, N.O. Wood, A "gentle" method for finishing Si3N4 balls for hybrid bearing applications, Tribol Lett, 7 (1999) 39-49.

[9] R.T. Lee, Y.C. Hwang, Y.C. Chiou, Lapping of ultra-precision ball surfaces. Part II. Eccentric V-groove lapping system, Int J Mach Tool Manu, 46 (2006) 1157-1169.

[10] R.T. Lee, Y.C. Hwang, Y.C. Chiou, Lapping of ultra-precision ball surfaces. Part I. Concentric V-groove lapping system, Int J Mach Tool Manu, 46 (2006) 1146-1156.

[11] R.T. Lee, Y.C. Hwang, Y.C. Chiou, Dynamic analysis and grinding tracks in the magnetic fluid grinding system Part II. The imperfection and ball interaction effects, Precis Eng, 33 (2009) 91-98.

[12] T.H.C. Childs, D.A. Jones, S. Mahmood, B. Zhang, K. Kato, N. Umehara, Magnetic

Fluid Grinding Mechanics, Wear, 175 (1994) 189-198.

[13] R.T. Lee, Y.C. Hwang, Y.C. Chiou, Dynamic analysis and grinding tracks in the magnetic fluid grinding system Part I. Effects of load and speed, Precis Eng, 33 (2009) 81-90.

[14] Y. Wu, W. Xu, M. Fujimoto, T. Tachibana, Ceramic Balls Machining by Centerless Grinding Using a Surface Grinder, Advances in Abrasive Technology Xiv, 325 (2011) 103-109.

[15] W. Xu, Y. Wu, M. Fujimoto, T. Tachibana, A new ball machining method by centreless grinding using a surface grinder, International Journal of Abrasive Technology, 5 (2012) 107-118.

[16] W. Xu, Y. Wu, A new in-feed centerless grinding technique using a surface grinder, J Mater Process Tech, 211 (2011) 141-149.

[17] W. Xu, Y. Wu, A new through-feed centerless grinding technique using a surface grinder, J Mater Process Tech, 211 (2011) 1599-1605.

[18] W. Xu, Y. Wu, T. Sato, W. Lin, Effects of process parameters on workpiece roundness in tangential-feed centerless grinding using a surface grinder, J Mater Process Tech, 210 (2010) 759-766.

[19] Y. Wu, T. Kondo, M. Kato, A new centerless grinding technique using a surface grinder, J Mater Process Tech, 162 (2005) 709-717.

[20] W. Rowe, M. Barash, Computer method for investigating the inherent accuracy of centreless grinding, International Journal of Machine Tool Design and Research, 4 (1964) 91-116.

[21] A.J.L. Harrison, T.R.A. Pearce, Reduction of lobing in centreless grinding via variation of set-up angles, Advances in Abrasive Technology Vi, 257-258 (2004) 159-164.

[22] W. Rowe, M. Barash, F. Koenigsberger, Some roundness characteristics of centreless grinding, International Journal of Machine Tool Design and Research, 5 (1965) 203-215.

[23] D. Barrenetxea, J. Alvarez, J.I. Marquinez, I. Gallego, I.M. Perello, P. Krajnik, Stability analysis and optimization algorithms for the set-up of infeed centerless grinding, International Journal of Machine Tools and Manufacture, 84 (2014) 17-32.

[24] W.B. Rowe, Rounding and stability in centreless grinding, International Journal of Machine Tools and Manufacture, 82 (2014) 1-10.

[25] P. Krainik, R. Drazumeric, B. Meyer, J. Kopac, C. Zeppenfeld, Simulation of workpiece forming and centre displacement in plunge centreless grinding, Int J Mach Tool Manu, 48 (2008) 824-831.

[26] Y. Furukawa, M. Miyashita, S. Shiozaki, Vibration analysis and work-rounding mechanism in centerless grinding, International Journal of Machine Tool Design and Research, 11 (1971) 145-175.

Vitae

Dr. Weixing Xu

Weixing Xu is a Research Fellow in the School of Mechanical and Manufacturing Engineering, The University of New South Wales, Australia. He received his Master of Engineering in Mechanical Engineering from Dalian University of Technology, China and PhD in Precision Engineering from Akita Prefectural University, Japan. His research has focused on ultrasonic vibration-assisted machining and laser machining.

Dr. Dandan Cui

Dandan Cui is a Postdoctoral Research Fellow working in the School of Mechanical & Mining Engineering, The University of Queensland, Australia. She got her PhD degree from the School of Mechanical and Manufacturing Engineering, The University of New South Wales, Australia. Her research is mainly focused on simulation of micro-/nano-machining and investigating the machining mechanism.

Dr. Yongbo Wu

Yongbo Wu is a Professor at the Department of Machine Intelligence and Systems Engineering, Akita Prefectural University, Japan. He received his Master of Engineering in Manufacturing Technology from Beijing University of Aeronautics and Astronautics, China, and PhD in Precision Engineering from Tohoku University, Japan. His research has focused on untraditional precision machining including ultrasonic vibration-assisted machining and magnetic field-assisted finishing.

Highlights

- First studied sphere forming mechanism in vibration-assisted ball centreless grinding
- Developed a 3D model for simulating vibration-assisted ball centreless grinding
- Confirmed vibration-assisted ball centreless grinding has high accuracy & efficiency
- Identified the rhythmical romation motion is critical for ball centreless grinding